Water Research 261 (2024) 122061

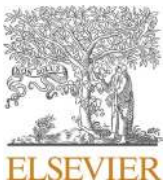

Contents lists available at ScienceDirect

Water Research

journal homepage: www.elsevier.com/locate/watres

Geometric relationship between the projected surface area and mass of a plastic particle

Tomoya Kataoka [a,b,*], Yota Iga [a], Rifqi Ahmad Baihaqi [c], Hadiyanto Hadiyanto [c], Yasuo Nihei [d,e]

[a] Department of Civil & Environmental Engineering, Ehime University, Matsuyama, Japan
[b] Center for Marine Environmental Studies, Ehime University, Matsuyama, Japan
[c] School of Postgraduate Studies, University Diponegoro, Semarang, Indonesia
[d] Department of Civil Engineering, Tokyo University of Science, Noda, Japan
[e] Research Center for Multi-hazard Urban Disaster Prevention, Research Institute for Science and Technology, Tokyo University of Science, Noda, Japan

ARTICLE INFO

Keywords:
Geometric relationship
Mass estimation
Projected surface area
Mesoplastics
Microplastics
River

ABSTRACT

The quantification of the mass of *meso*/microplastic (MMP) particles is crucial for assessing the global inventory of ocean plastics and assessing environmental and human health risks. Herein, linear regression models between mass and projected surface area on a log scale were established by directly measuring the masses of 4390 MMP particles collected at 35 sites in 17 Japanese rivers with an ultramicrobalance. The linear regression models estimated mass concentrations more accurately than any previous method based on geometric volume assuming several three-dimensional shapes. Additionally, linear regression models were quite reasonable for determining the geometric relationships of idealized cuboid particles. The slope of the linear regression models was dependent on the three-dimensional shapes of the particles, and their intercept was determined according to their third dimension. Moreover, the third dimension led to uncertainty in the mass estimation of particles; thus, the accuracies of the previous methods were relatively poor. Nevertheless, two limitations for mass measurement by linear regression models were identified, which determined the size range of the MMP particles on the projected surface area (ranging from 10^{-4} mm^2 to 10^2 mm^2) that is applicable for mass estimation of the particles collected from riverine and marine environments. Our results could be used to accurately estimate the mass concentrations in aquatic environments and provide insights into the geometric relationships between the mass and size of MMP particles.

1. Introduction

The contamination of aquatic environments (e.g., oceans, rivers, and lakes) with mesoscale (5–25 mm in size) and microscale (<5 mm in size) plastic (MMP) particles has been evaluated in units of m^{-3} (particle count per unit water volume) or km^{-2} (particle count per unit area) with surface net towing, water pumping, and bulk sampling techniques (Isobe et al., 2021). The level of contamination is referred to as the numerical concentration. The numerical concentration is significant for comparing microplastic contamination among environments and discussing the behaviors of particles in water columns; it can quantify MMPs with mass concentrations to assess the global inventory of ocean plastics (Koelmans et al., 2017; Thompson et al., 2004) and assess risks to the environment and human health (Koelmans et al., 2022). To gain more information from laboratory tests for risk assessment, effect concentrations should be reported more accurately and explicitly in terms of both mass and numerical concentrations (de Ruijter et al., 2020). For instance, to facilitate the development of human-health risk assessments and effective management and policy options, the global average rate of microplastics ingested (g/year/person) has been estimated as the product of the average number of microplastics ingested (particles/year/person) and the average mass of individual MMP particles (g/particles) (Senathirajah et al., 2021). The geometric volume of an MMP particle is also a relevant dose metric for a food dilution mechanism (de Ruijter et al., 2020). The individual MMP mass can often be a reasonable proxy for its geometric volume because the MMP mass is proportional to the volume, where the proportionality constant is the polymer density of the MMP particle (approximately 1.00 mg/mm^3) and is less variable than other microplastic characteristics, such as the particle size and shape (Koelmans et al., 2020, 2022;

* Corresponding author at: Department of Civil & Environmental Engineering, Ehime University, 3 Bunkyo-cho, Matsuyama, Japan, 790-8577.
E-mail addresses: kataoka.tomoya.ab@ehime-u.ac.jp, tkata@cee.ehime-u.ac.jp (T. Kataoka).

https://doi.org/10.1016/j.watres.2024.122061
Received 27 February 2024; Received in revised form 15 May 2024; Accepted 6 July 2024
Available online 8 July 2024

Redondo-Hasselerharm et al., 2018). Hence, the particle count can be converted into particulate mass based on the assumption of shape and identification of the polymer materials comprising individual MMP particles (Cózar et al., 2014; Isobe et al., 2019; Kooi et al., 2016; Pabortsava and Lampitt, 2020; Simon et al., 2018).

A basic approach for converting particulate mass (M) is to calculate the geometric volume (V) of the MMP particle and to multiply its polymer density (ρ) by this volume (i.e., $M = \rho V$). The densities of the major polymer materials are shown in Table S1. Nevertheless, the polymer density of environmental MMP particles can differ greatly from the density of pure polymers because of differences in molecular mass, crystallinity, and additives used in plastic production (Andrady, 2017). Moreover, the geometric volume of individual particles has rarely been measured with X-ray tomography (Sagawa et al., 2018; Tötzke et al., 2021) because of the time-consuming nature of the technique; thus, their three-dimensional shape, especially the third dimension (thickness or height), is unknown (Mintenig et al., 2018). Instead, two dimensions and an area and on a projected plain have been determined. In general, the first dimension is the length of the major axis, and the second dimension is the length of the minor axis, which is perpendicular to the major axis. The projected surface area is determined by viewing individual particles perpendicularly. Nonetheless, uncertainty exists in the determination of particulate mass from the three-dimensional shape of MMP particles.

Thus, several researchers have estimated the geometric volume of individual particles by assuming that their three-dimensional shapes can be classified into four specific shapes: spheres, ellipses, cylinders, and flakes (Pabortsava and Lampitt, 2020). The three-dimensional shape is assumed to be a sphere by transforming the irregularly shaped particles into circles with projected surface areas that are equivalent to their real area (Kooi et al., 2016; Yokota et al., 2017). Since the particles are reshaped into spheres, the third dimension is not needed when determining the geometric volume. Some studies have assumed that the shape is an ellipsoid (Poulain et al., 2019; Simon et al., 2018). The ellipsoidal model requires additional assumptions regarding the third dimension. Poulain et al. (2019) assumed that the third dimension is equal in size to the minor-axis length. Moreover, Simon et al. (2018) reported that the aspect ratio of the third dimension to the minor-axis length is equivalent to that of the minor-axis length to the major-axis length. The other assumption is that the three-dimensional shape is a cylinder (Isobe et al., 2019). The cross-sectional area of the cylinder is determined by the base diameter corresponding to the length of the major axis, and the cylinder height is varied by multiplying the base diameter by an adjustable constant (Isobe et al., 2019). The fourth assumption is to consider particles as flat fragments or flakes (Cózar et al., 2014). The geometric volume is determined by the cube of the major-axis length and a factor corresponding to a flat-shaped volume. The details of these methodologies are discussed in Section 3.3. Regardless, in all cases, the geometric volume is uncertain due to its unknown third dimension. Furthermore, the accuracy of the estimated mass is strongly dependent on the actual three-dimensional shape.

Herein, to evaluate the uncertainty in these previous methodologies, we reveal the geometric relationship between the size and mass of microplastics based on their mass measured using an ultramicrobalance (Kataoka et al., 2019; Nihei et al., 2020). In particular, we clarify that the projected surface area is an important parameter for determining the MMP mass. The geometric relationship is theoretically explained by assuming the shape and polymer density of the MMP particles. Furthermore, the applicability of the geometric relationship to the estimation of mass concentration is discussed. This technique is compared with the previous mass estimation method based on the geometric volume of an assumed three-dimensional shape (volume-based method). This research provides guidance for accurately estimating mass concentrations in aquatic environments and provides insights into the geometric relationship between size and mass.

2. Materials and methods

2.1. Meso/microplastic sampling

A total of 35 MMP sampling sites were selected in 17 Japanese rivers (Fig. 1) from May 2019 to October 2022 (Table S2). The sampling surveys were conducted during periods without precipitation. These sites were selected from urban and rural areas to consider the effects of load on human activity (Kataoka et al., 2019). Thus, the ratio of an urban area to a river basin (the urban area ratio) ranged between 0.1 % and 82 %, and the population density ranged between 0.4 and 6067 persons km^{-2} (Table S2).

The conical and square pyramid types of plankton nets, each with a 335-μm mesh size, were employed for the surveys. The conical net was 30 cm in diameter, 75 cm in length, and 0.45 in gauze porosity, which was the same material as that used in our previous works (Kataoka et al., 2019; Nihei et al., 2020). This method was used for net sampling in the Kanto region until 2020 (i.e., 1a−4; see Fig. 1 and Table S2). Moreover, the width, height, length, and porosity of the square pyramid net were 50 cm, 30 cm, 130 cm, and 0.45, respectively. This method has been used for net sampling in the Shikoku region since 2021 (i.e., 5a−17; see Fig. 1 and Table S2). The open area ratio of the nets is the ratio of the gauze surface area (s) times the porosity (β) to the projected net mouth area (a) (i.e., $s\beta/a$); the ratios of the conical and square pyramid nets were 2.41 and 2.63, respectively (Kataoka et al., 2023). A flow meter with a speed range of approximately 0.06–1 m/s (2030R6, General Oceanics Inc., USA) was attached to the net mouths.

The net sampling surveys at the sites of 15 rivers, excluding the Ohori and Toneunga Rivers, were conducted on bridges by hanging the net at the center of the stream. The sampling duration was shorter than 10 min (usually 5 min) to avoid clogging (Kataoka et al., 2023). Moreover, net sampling surveys of the Ohori and Toneunga Rivers were conducted to investigate the variance and confidence intervals of the MMP data and the effect of clogging when filtering fresh water for river MMP sampling (Kataoka et al., 2023; Tanaka et al., 2022; 2023). In the sampling experiment, the conical net was fixed on the surface by three 1.2-m-long steel stakes to prevent vertical and horizontal swaying (Kataoka et al., 2023; Tanaka et al., 2022; 2023). The sampling duration ranged between 3 min and 30 min to examine the clogging effect (Kataoka et al., 2023). After all the samples were collected, the net mouth was covered with a customized cover, and the net was returned to the laboratory.

As noted above, there were differences in tools and methodologies for net sampling surveys. This difference could yield unexpected uncertainties and variances in the MMP concentration data and make it difficult to compare the MMP abundance data(Michida et al., 2019). Nonetheless, the differences in sampling tools and methods were disregarded in the present study because we focused on the characteristics of MMP particles, not MMP abundance.

2.2. Laboratory analysis for identifying meso/microplastics

In addition to the differences in sampling tools and methodologies, it was essential to harmonize the protocol of laboratory analyses to investigate the characteristics of MMP particles. Thus, we identified the MMP from each sample by applying the following methodology, which we adopted in our previous studies (Kataoka et al., 2023; Nihei et al., 2020; Tanaka et al., 2022; 2023).

After the net sampling surveys, the net was rinsed with tap water filtered through a 100-μm mesh nylon net. Then, all materials collected by the net were temporarily transferred to 500-mL stainless steel bottles with rinsed water. Then, the samples were filtered with a 100-μm nylon net, placed on a glass Petri dish with a glass lid, and dried at 60 °C for at least 24 h. The dried samples were transferred to a 100-mL glass beaker. In addition, 50 mL of a 30 % hydrogen peroxide (H_2O_2) solution was poured into the beaker to oxidatively degrade natural organic matter at room temperature (approximately 20 °C) for at least one week. A total of

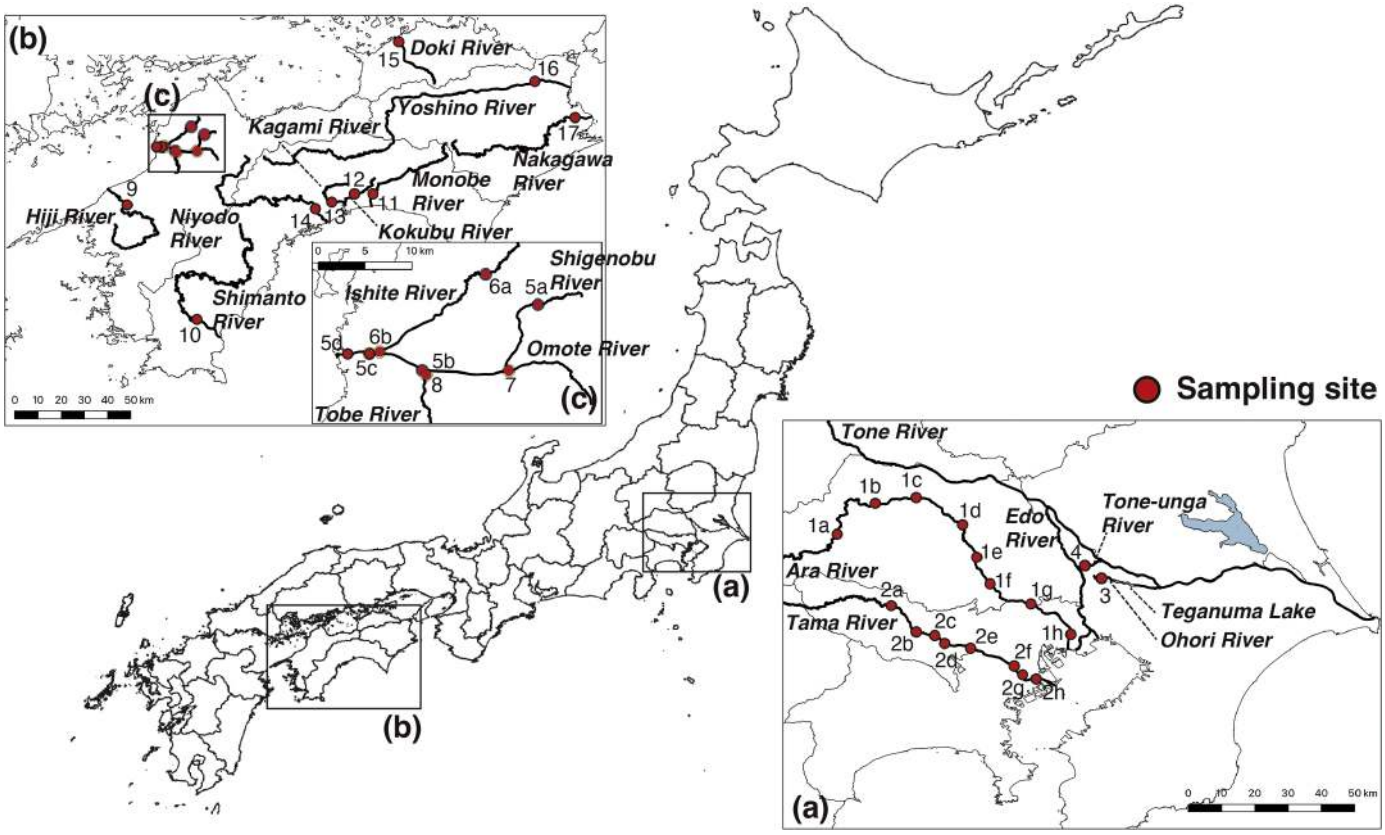

Fig. 1. Locations of the sampling sites and rivers: (a) Kanto region, (b) Shikoku Island, and (c) an enlarged map of the Shigenobu River basin. The site numbers are the "Site ID" in Table S2. The river names are shown.

50 mL of 30 % H_2O_2 aqueous solution containing 5 mL of $FeSO_4$ (50 mmol/L) was added to several samples collected from the Shigenobu River in 2022 (5a–5c and 6a–8; Table S1) to facilitate oxidative digestion through the Fenton reaction. Oxidative digestion through the Fenton reaction was performed at room temperature for three days. The Fenton reaction did not affect polymer chemistry or size (Tagg et al., 2017); thus, the difference in the oxidative degradation process was neglected. After oxidative degradation, the residual matter was again filtered through a 100-μm nylon net and subsequently dried at 60 °C for at least 24 h.

Two different analysts picked up particles that resembled MMP particles from residual matter with steel use stainless (SUS) tweezers through visual observation (Hidalgo-Ruz et al., 2012). The mass of each particle was measured using an XPR Ultramicrobalance (XPR2UV, Mettler Toledo Co. Ltd., Japan) with maximum capacity and readability of 2.1 g and 0.1 μg, respectively. The resolution of the ultramicrobalance is determined by the ratio of readability to maximum capacity, that is 1/21,000,000. The minimum weight with 1 % of tolerance is 0.03 mg, and thus the uncertainty in mass could occur in measuring mass lighter than 0.03 mg. Then, images of each particle were recorded with a stereoscopic microscope (SZX7, Olympus Co. Ltd., Japan) equipped with a universal serial bus (USB) camera (HDCE-20C; AS ONE Co. Ltd., Japan) for subsequent size measurements. Based on the particle images, the particles were categorized into five shapes: pellets, spheres, fragments, fibers, and sheets. Then, the polymer type of each particle was identified by Fourier transform infrared (FTIR) spectroscopy (IRAffinity-1S, Shimadzu Co. Ltd., Japan) with attenuated total reflection (ATR) equipment (Quest, Specac Ltd., Japan). The infrared (IR) absorption spectrum was measured by scanning from 500 to 4600 cm^{-1} at a resolution of 4 cm^{-1}, which was obtained from three libraries containing the reference IR spectra of various polymers (ATR-Polymer2, Irs-Polymer2, and T-Polymer2 provided by Shimadzu Co. Ltd.). The hit quality index (HQI) ranged from 0 to 1000 ‰; thus, we set 700 ‰ HQI as the threshold value to avoid polymer-type misidentifications. All the MMP particles were categorized into nine polymer types (Table S1).

Finally, the length of each MMP particle on the major axis (major length) and the projected surface areas of all MMP particles were measured using ImageJ (https://imagej.nih.gov/ij/). The major length (i.e., first dimension) was used to represent the size of the MMP particle (GESAMP, 2019). According to previous reports, all particles were categorized into mesoplastics (5–25 mm) and microplastics (<5 mm) with specified major lengths. To reduce the uncertainty in the MMP size associated with the other dimensions, the minor length (i.e., the second dimension) and projected surface area were measured. Individual MMP particles were placed with the most stable plane under a stereoscopic microscope. The projected area of the top surface was defined as the plane with the maximum area of particles. The minor length was calculated by dividing the projected surface area by the major length, which corresponds to the mean length along an axis orthogonal to the major axis. Unfortunately, we could not reliably measure the height along the vertical axis of the top surface (i.e., the third dimension). Consequently, these two size parameters were used to explore the relationship with the mass of the MMP particles in a subsequent regression analysis and to evaluate the accuracy of the previous volume-based method for mass estimation.

2.3. Quality control and quality assurance

Several quality control procedures were performed during the field surveys and laboratory analyses. The mouth of the net was covered with 100 % cotton cloth before and after sampling. The tap water used to rinse the net was filtered through a 100-μm nylon net. The 100-μm nylon net was washed with pure water before use. Since nylon nets were used during sampling and laboratory analysis, 149 nylon particles identified

by FTIR analysis were excluded. During the laboratory analyses, we wore 100 % cotton robes and avoided plastic instruments (e.g., beakers, Petri dishes, and tweezers). In addition, airborne contamination was examined by collecting particles deposited on disposable Petri dishes (φ91 mm) on tables through laboratory analyses. FTIR was used to analyze the deposited particles, identifying those materials under the same IR spectrum libraries. As a result, 11 contaminated plastic particles were observed in 7 of 35 samples. After these particles were cross-examined for the color, shape and polymer type of each plastic particle in the same sampling group, no questionable plastic particles were observed, indicating that no unexpected plastic contamination occurred during the laboratory analyses.

2.4. Statistical analyses

A linear regression analysis was conducted to determine the relationship between the projected surface area (S) and particulate mass (M) of the MMP particles. As there were considerable variations in both M and S, a linear regression analysis was performed on the ordinary logarithms of M and S as follows:

$$\log_{10}M = b\log_{10}S + a \quad (1)$$

where a and b are regression coefficients that were determined by the least squares method. Eq. (1) was transformed to $M = 10^a S^b$. The model performance was evaluated on the basis of the coefficients of determination (r^2) and the expected value of the residual ($\bar{s}$) defined below:

$$\bar{s} = \sqrt{\frac{\sum \left(\log_{10}M_e - \log_{10}M_o\right)^2}{N_p - 2}} \quad (2)$$

where M_e and M_o are the estimated and measured masses of individual MMP particles, respectively, and N_p is the number of MMP particles used to develop the linear regression models.

Furthermore, the mass concentrations at the 35 sites (C_e) were estimated by applying the regression model and compared to the measured concentrations (C_o). *Bias* and the root mean square error (*RMSE*) were evaluated based on the following equations:

$$Bias = \overline{C}_e - \overline{C}_o \quad (3)$$

$$RMSE = \sqrt{\frac{1}{N_s}\sum \left(C_e - C_o - Bias\right)^2} \quad (4)$$

where $\overline{C}_e$ and $\overline{C}_o$ are the geometric means of the estimated and measured mass concentrations, respectively. These statistical parameters (*Bias* and *RMSE*) are often utilized in oceanography and meteorology to evaluate estimation errors by dividing them into systematic and random components (Iwasaki, 2023). Notably, the geometric means were calculated because the variance in the mass concentration was overly large. N_s is the total sampling frequency at the 35 sites, and its value was 66 in this study (Table S2). Furthermore, to examine the nonparametric correlation, Spearman's rank correlation coefficient (r_s) was evaluated. The python package scipy (ver 1.4.1) was used throughout all the statistical analyses.

3. Results

3.1. Compositions of the shapes and polymers of meso/microplastic particles

The total number and mass of the MMP particles were 4390 and 676 mg, respectively. The size distributions indicated that mesoplastics accounted for only 6 % of the total MMP particles, while microplastics accounted for 94 % (Fig. 2). Nevertheless, 39 % of the total mass was mesoplastics, and 61 % was microplastics (Fig. 2), indicating the importance of quantifying mesoplastics in the river environment to determine the plastic load to the ocean and/or mass balance between plastic production and waste (Nihei et al., 2024). The fragmented particles accounted for 69.6 % of the total number of MMP particles, and the percentage of fibrous particles was 27.7 % (Figure S1). The two shapes were predominant in terms of plastic contamination in Japanese rivers, accounting for 97.3 % of the total. Many of the fragmented particles were polypropylene (PP) (39 %) and polyethylene (PE) (21 %) (Figure S1). Moreover, the fibrous particles were mostly polyester/polyethylene terephthalate (PEs/PET) (17 %) and PP (7.4 %).

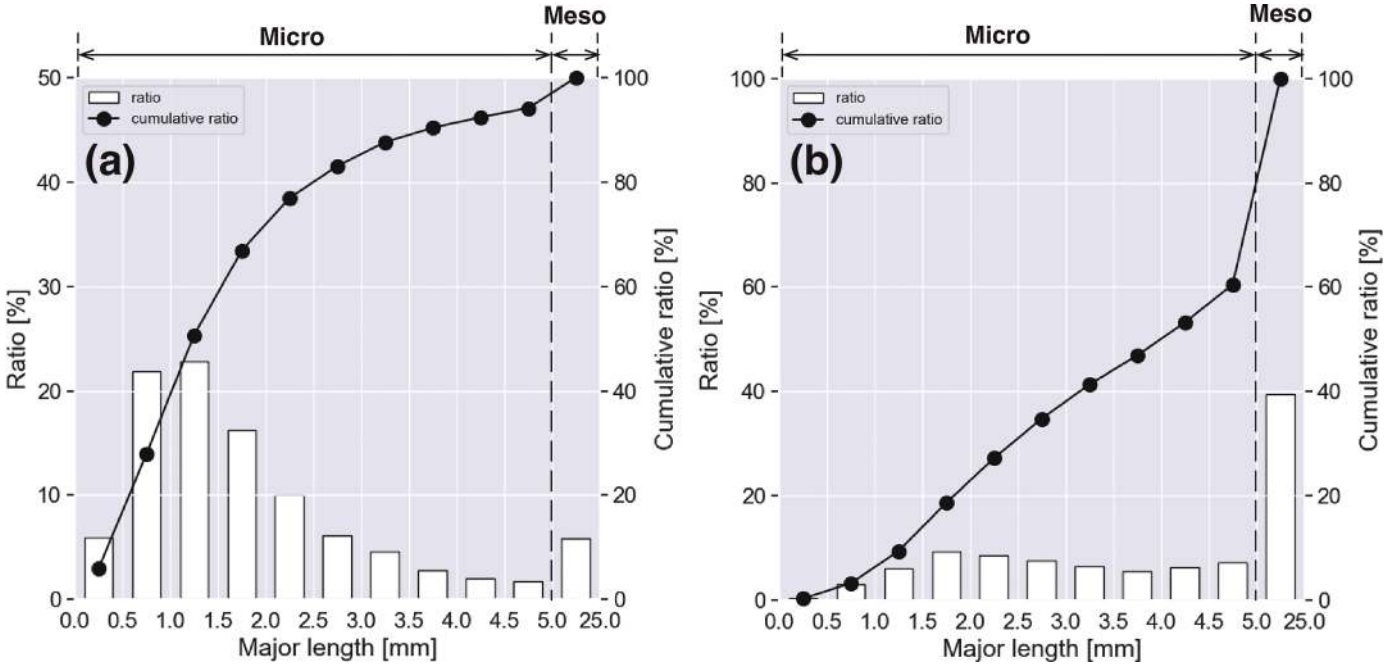

Fig. 2. Size distributions of the number (a) and mass (b). The legends are shown in the upper right box of each panel. The broken vertical line indicates the size boundary between *meso*/microplastics.

Moreover, the masses of the plastic particles significantly differed from the numbers. A total of 92.5 % of the total mass was fragmented particles, while fibrous particles accounted for only 2.3 %, which was lower than that of the sheet-form particles (4.6 %).

3.2. Relationship between the size and mass of meso/microplastic particles

To correlate the size and mass of the *meso*/microplastic particles, the regression coefficients a and b in Eq. (1) were determined by the least squares method (the regression line is the red solid line in Fig. 3a). The regression coefficients were $a = -1.12 \pm 0.01$ and $b = 1.14 \pm 0.01$ ($N_p = 4390$; $R^2 = 0.76$). a, which is the intercept of Eq. (1), is the mass of the plastic particle when $S = 10^0$ mm^2. The parameter b is the slope of Eq. (1), which is the gradient of $\log_{10}M$ against $\log_{10}S$. $b \approx 1$ indicates that M could become one order of magnitude greater when S increased by one order of magnitude. The expected value of the residual $\bar{s}$ was 0.40 (Table 1); thus, according to Eq. (2), the range of variation of $\frac{M_e}{M_o}$ was $10^{\pm 0.40}$. The variance in M would depend on the third dimension, polymer type (or density) and shape. Note that $M < 0.03$ mg (minimum weight with 1 % of tolerance) could contain the uncertainty in measuring the mass (see 2.2). Nevertheless, the regression analysis demonstrated that the mass of the MMP particles was significantly associated with the projected surface area.

3.3. Comparison of linear regression models for particles with different shapes and polymer types

To discuss the differences among shapes and polymer types, the parameters a and b were calculated using the projected surface area and mass data (Table 1). The parameter a varied depending on the shape type, and the values were in the following ascending order: spherical, fragmented, sheet-form, and fibrous particles. Fibrous particles were the lightest among all the shapes. Moreover, the parameter b of the spherical particles was the greatest, and that of the fibrous particles was the lowest. Interestingly, the b values of the shape types, excluding fibrous particles, were greater than 1. As 62 % of the fibrous particles were PE/PET (Figure S1), the parameter b of these particles was lower than that of the particles composed of other polymers.

Excluding the linear regression models developed using fewer than 50 data points (Table 1), the expected values of the residual $\bar{s}$ were approximately 0.4, similar to the results obtained for all particles, which ranged from 0.36 to 0.43 (Table 1). This finding indicated that it was not critical to categorize the shape and polymer type when applying the regression equation (Eq. (1)). In other words, this suggests that the coefficients estimated from the data of all the particles (Table 1) were applicable regardless of the shape and polymer type.

Table 1
Regression coefficients were determined by the least squares method.

	N_p	a	b	R^2	$\bar{s}$
All	4390	−1.12 ±0.01	1.14 ±0.01	0.76	0.04
Each shape					
Sphere	8	−0.49 ±0.06	1.17 ±0.08	0.97	0.13
Fiber	1216	−1.62 ±0.03	0.82 ±0.02	0.58	0.37
Fragment	3052	−1.05 ±0.01	1.13 ±0.01	0.71	0.43
Sheet	113	−1.31 ±0.04	1.10 ±0.07	0.67	0.39
Each polymer					
Polyethylene (PE)	989	−0.99 ±0.01	1.21 ±0.02	0.74	0.40
Polypropylene (PP)	2115	−1.11 ±0.01	1.13 ±0.02	0.71	0.36
Polystyrene (PS)	42	−1.24 ±0.06	1.04 ±0.15	0.56	0.35
Polypropylene and Polyethylene copolymer (PEPP)	158	−1.16 ±0.04	1.14 ±0.06	0.73	0.37
Polyvinyl chloride (PVC)	13	−0.69 ±0.10	1.56 ±0.16	0.90	0.22
Polyester/Polyethylene terephthalate (PEs/PET)	802	−1.74 ±0.04	0.76 ±0.03	0.51	0.42
Polymethyl methacrylate (PMMA)	19	−1.17 ±0.13	1.10 ±0.11	0.85	0.35
Ethylene vinyl acetate (EVA)	35	−1.14 ±0.11	1.24 ±0.14	0.71	0.51
Other	215	−1.31 ±0.04	0.89 ±0.04	0.73	0.42

3.4. Applicability of the linear regression model to the estimation of mass concentration

The mass concentrations at 35 sites were first estimated by linear regression models (Eq. (1)) to demonstrate their applicability and then compared to the actual values measured by the ultramicrobalance (Fig. 4). The MMP masses were estimated by regression models established from all particle data (*Model* 0), only shape-related particle data

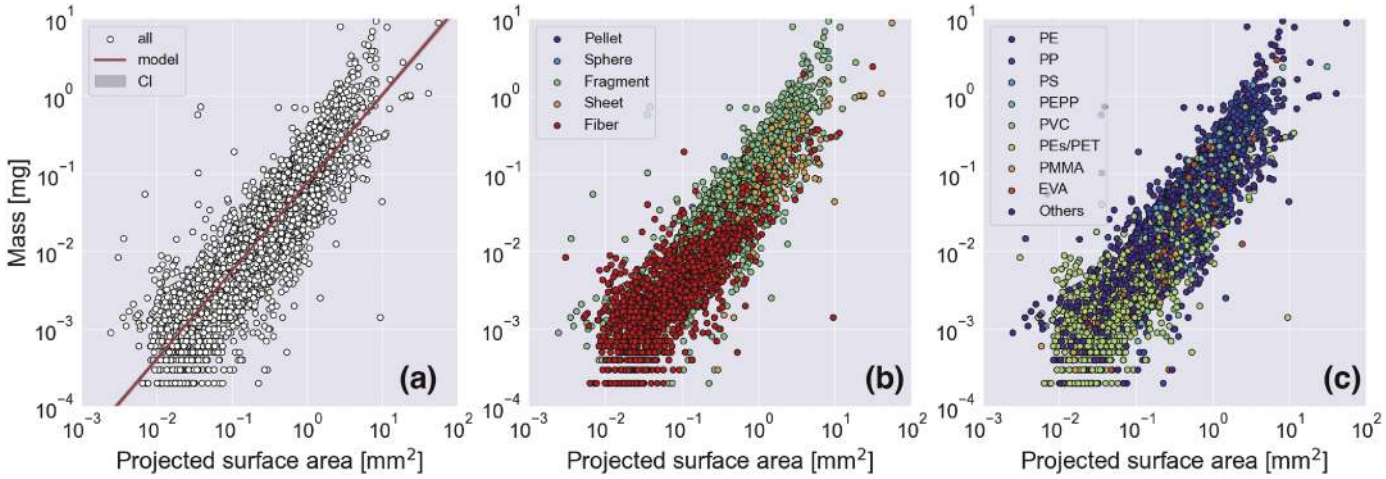

Fig. 3. Regression analysis between mass and projected surface area of all particles (a), each shape-type particle (b), and each polymer-type particle (c). In panel (a), the linear line regressed by Eq. (3) is shown as a solid red line with a light gray area representing the 95 % confidence interval. The legends are shown in the upper right box of each panel.

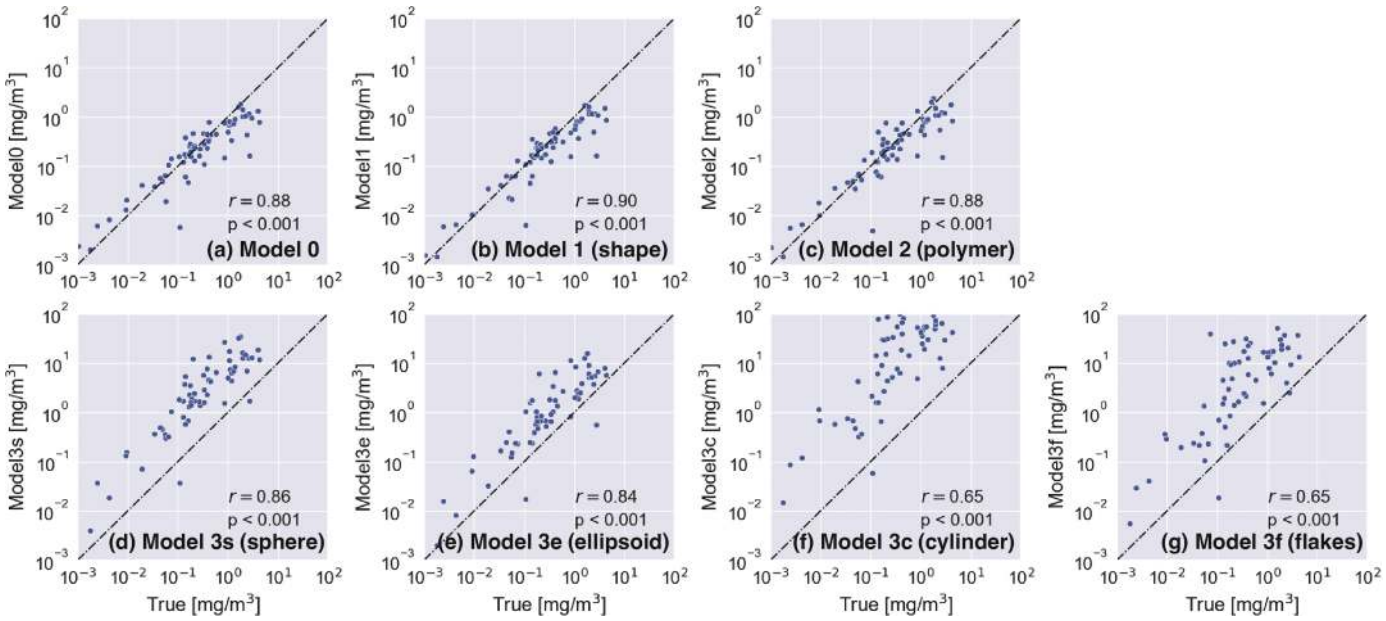

Fig. 4. Correlation between the measured and estimated mass concentrations. Comparisons of the results estimated by our regression models are shown in the upper panels ((a) Model 0, (b) Model 1, (c) Model 2), while those estimated by the volume-based methods are shown in the lower panels ((d) Model 3 s, (e) Model 3e, (f) Model 3c, (g) Model 3f). The Spearman's rank correlation coefficient and statistical significance characteristics are shown in each panel.

(*Model* 1) and only polymer-related particle data (*Model* 2) (Figure S3); then, the total MMP mass at each of 66 samplings (see Table S2) was normalized to the sample volume. The MMP masses estimated by all regression models were very consistent with the measured masses (Figure S3), and consequently, the mass concentrations were in good agreement with the measured concentrations (Figs. 4a, 4b and 4c). The results of Model 1 and Model 2 were not significantly different from those of Model 0, suggesting that the categorization of the shapes (*Model* 1) and polymer types (*Model* 2) had little effect on the estimation of mass concentration (Figures S3 and 4).

To compare the performances of the linear regression models, the mass concentrations were estimated by assuming four three-dimensional shapes (spheres, ellipsoids, cylinders, and flakes) based on Pabortsava and Lampitt (2020) (i.e., volume-based methods). When assuming a spherical particle, the geometric volume was defined by

$$V_s = \frac{1}{6}\pi D_s^3 \tag{5}$$

where D_s was determined by an equivalent diameter calculated from the projected surface area (S_s) measured in the present study; that is, $D_s = \sqrt{4S_s/\pi}$. Assuming an ellipsoidal particle, the geometric volume was

$$V_e = \frac{1}{6}\pi d_1 d_2 d_3 \tag{6}$$

where d_2 and d_3 are the measured minor-axis lengths and d_1 is the measured major-axis length (e.g., Poulain et al., 2019; Simon et al., 2018). Assuming a cylindrical particle, the geometric volume was calculated by

$$V_c = A_c \gamma d_1 \tag{7}$$

where $A_c = \frac{\pi d_1^2}{4}$ is the cross-sectional area and γ is an adjustable constant, which was selected as 0.4 following Isobe et al. (2019). Assuming a fragmented particle, the geometric volume was calculated by

$$V_f = \alpha d_1^3 \tag{8}$$

where α was determined to be 0.1 according to Cózar et al. (2014). However, if the MMP particle is fibrous, these methodologies could be inappropriate because the three-dimensional shape is quite different. Thus, the geometric volume of fibrous MMP particles was calculated according to the methodology of V_c, regardless of any assumptions. Finally, the mass of each MMP particle was estimated by multiplying the polymer density ρ by the geometric volume (V_s, V_e, V_c, and V_f), which are referred to as *Model* 3_s, *Model* 3_e, *Model* 3_c, and *Model* 3_f, respectively.

Then, the mass concentrations at 35 sites estimated by these volume-based methods for mass estimation were compared to the measured values (Figs. 4d–4g). Overall, these mass concentrations were over-estimated compared with the measured concentrations despite the high rank correlation coefficient (Figs. 4d–4g). The bias and RMSE of the mass concentration estimated by the volume-based methods were significantly greater than those estimated by our regression models (Table 2). This is because the heavier the MMP masses were, the larger the errors yielded (Figure S3). This finding indicated that the volume-based methods tended to overestimate the mass concentration, resulting from the uncertainty of the third dimension. Hence, it was necessary to evaluate the third dimension more appropriately when estimating the mass with volume-based methods.

4. Discussion

Our research revealed three significant findings. (1) The projected surface area (S) was linearly related to the mass of the MMP particles (M)

Table 2
Accuracies of the mass concentrations estimated by our method and by the volume-based method.

	Bias [mg/m³]	RMSE [mg/m³]	r_s	N_s
Our study				
Model 0	−0.054	0.77	0.88	66
Model 1	−0.062	0.74	0.90	66
Model 2	−0.044	0.74	0.88	66
Volume-based method				
Model 3s	1.667	7.86	0.86	66
Model 3e	0.591	3.19	0.84	66
Model 3c	9.536	95.41	0.65	66
Model 3f	3.131	30.17	0.65	66

(Fig. 3). (2) The variance in M was similar regardless of the shape and polymer type (Table 1). (3) Eq. (1) could be estimated more accurately than the previous volume-based models, and the latter would overestimate the mass concentration due to uncertainty in the third dimension (Fig. 4). Herein, we discuss the following aspects: (1) Why is S linearly related to M? (2) How large is the variance in M depending on the difference in shape and polymer type? (3) Finally, the applicability and limitations of these methods are discussed.

For discussion, we assume that the three main orthogonal dimensions can be provided by $d_1 \geq d_2 \geq d_3$. If a particle can be described by a sphere or a cube, all of these dimensions are equal: $d_1 = d_2 = d_3$. In general, S is determined by d_1 and d_2, and thus, the third dimension corresponds to d_3. The geometric volumes of all particulate shapes can be calculated from these orthogonal dimensions by assuming several morphologies.

4.1. Linear relationship between the projected surface area and mass on a log scale

The M of a plastic particle is geometrically determined by the density of its polymer material (ρ) (≈ 1.00 mg/mm^3) and its geometric volume (V) (i.e., $M = \rho V$). V and S can be defined according to the shape, and these geometric relationships can be derived (Table 3). These relationships are commonly converted into log-scale equations:

$$\log_{10} M = \log_{10}\alpha + \log_{10} S \tag{9}$$

where α is derived from the geometric relationship (Table 3). For instance, $\alpha = \frac{2}{3}\rho d_3$ for a sphere. Compared to Eq. (1), $b = 1$ and $a = \log_{10}\alpha$ are likely to be expressed regardless of the shape.

Based on the comparison, the estimated a should be dependent on the third dimension (d_3) because $\rho \approx 1.00$ mg/mm^3. To verify this assumption, the d_3 of each particle collected by net sampling can be estimated by the geometric relationship of each shape between the measured M and S (Figure S4). For example, for a spherical particle, d_{3e} can be calculated by $\frac{3M}{2\rho S_s}$ based on Table 3, where ρ depends on the polymer type identified by FTIR (Table S2). Consequently, the estimated third dimension d_{3e} is in the range of 10^{-2} to 10^{0} mm (Figure S4), and its geometric mean d_{3e} for fibrous particles is the thinnest (Table 3). $\log_{10}\alpha$ of Eq. (9) is evaluated by using the geometric mean of d_{3e}. Interestingly, $\log_{10}\alpha$ is consistent with the estimated a of Eq. (1) shown in Table 1, demonstrating that d_{3e} is more important than ρ for determining the intercept of Eq. (1). In other words, it is important to consider the shape rather than the polymer type when estimating M. In fact, M estimated by *Model* 1 is slightly greater than *Model* 0 (Fig. 4 and Figure S3).

In principle, the slope b varies between 1 and 1.5 depending on morphological characteristics. Assuming that the three main orthogonal dimensions can be provided by $d_1 \geq d_2 \geq d_3$, the range of b is derived from the gradient of $M'(=\log_{10} M)$ and $S'(=\log_{10} S)$. If a particle can be described by a circle or cube, $b = \frac{dM'}{dS'} \approx 1.5$ because M and S are proportional to d_1^3 and d_1^2, respectively, when the three orthogonal dimensions are equal (i.e., $d_1 = d_2 = d_3$). In contrast, M is proportional to S when assuming that the third dimension (d_3) is constant; hence, $b = \frac{dM'}{dS'} \approx 1.0$. In fact, the estimated b is within this range except for *Model* 1 for the fibrous material and *Model* 2 for the other materials, including PE/PET (Table 1). These particles with large projected surface areas (e.g., $S = 10^0 \sim 10^1$ mm^2) are rarely observed in the sampling data (Fig. 3b and 3c). Therefore, these regression models underestimate M in the range of large projected surface areas.

4.2. Variance in mass against the projected surface area

The variance in the mass over the projected surface area was relatively large and did not depend on the particle shape and polymer type (Table 1). As mentioned in Section 3.2, the variance could mainly depend on that in the third dimension. To demonstrate the reasonableness of the variance, the geometric relationship between the mass (M) and projected surface area (S) of the particles is considered by categorizing the particles into four basic shapes: 1D, 2D, 3D and IS (Figure S5; Rosal (2021)). A one-dimensional (1D) object, such as a fiber, is an object with a high aspect ratio. A two-dimensional (2D)

Table 3
Geometric relationship between the mass and projected surface area of each shape.

Shape	Schematic image	V	S	Relationship between M and S	Geometric mean of d_{3e} [mm]	$\log_{10}\alpha$ [*4]
Sphere [*1]	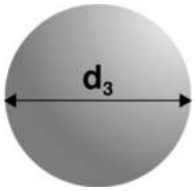	$V_s = \frac{\pi}{6} d_3^3$	$S_s = \frac{\pi}{4} d_3^2$	$M_s = \frac{2}{3}\rho d_3 S_s$	0.44	−0.53
Fiber [*2]	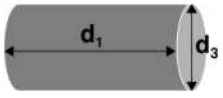	$V_f = \frac{\pi}{4} d_3^2 d_1$	$S_f = d_1 d_3$	$M_f = \frac{\pi}{4}\rho d_3 S_f$	0.038	−1.53
Fragment [*3] Sheet [*3]	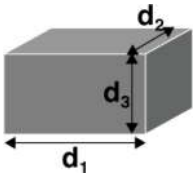	$V_c = d_1 d_2 d_3$	$S_c = d_1 d_2$	$M_c = \rho d_3 S_c$	0.083 0.055	−1.08 −1.26

[*1] As $d_1 = d_2 = d_3$, the diameter of the spherical particle is considered d_3.
[*2] Assuming that the fiberfibre is cylindrical, d_3 corresponds to its diameter, as the cross-sectional shape is a circle. d_1 denotes the length of the fibrous particle on a major axis. The projected shape of the cylindrical fiber is likely to be rectangular.
[*3] Assuming that the sample is rectangular, d_2 and d_3 denote the minor length and thickness of the fragmented or sheet particle, respectively.
[*4] $\log_{10}\alpha$ was evaluated based on the geometric mean of d_{3e} assuming that $\rho \approx 1.00$ mg/mm^3.

object is a relatively flat object, such as a plate or sheet. A three-dimensional (3D) object is an isometric object in which the sides are all equal, such as cubes and spheres. An intermediate-shaped (IS) object is any object outside the above three basic shapes, such as fragments.

The four basic shapes can be categorized by the three morphological parameters *equancy*, *platiness* and *elongation* according to Rosal (2021):

$$equancy = \frac{d_3}{d_1} \tag{10}$$

$$platiness = \frac{d_2 - d_3}{d_1} \tag{11}$$

$$elongation = 1 - \frac{d_2}{d_1} \tag{12}$$

where the three main orthogonal dimensions that satisfy $d_1 \geq d_2 \geq d_3$ are used to categorize the four basic shapes in the present study (Table S2). Notably, the sum of these three morphological parameters is 1. A particle is categorized as 1D if *platiness* is smaller than 0.5 and *elongation* is greater than 0.5 (Figure S5). Similarly, 2D (3D) can be determined by *equancy* and *platiness* (*equancy* and *elongation*); the boundary is shown by the broken line in Figure S5. If all three morphological parameters are less than 0.5, the particle is categorized as an IS.

Assuming a cuboid object with three dimensions (i.e., d_1, d_2, *and* d_3) between 0.01 mm and 25 mm based on the definition of *meso*/micro-plastics, the mass and the projected surface area can be calculated as M_c and S_c, respectively, as shown in Table 3. Notably, $\rho \approx 1.0$ mg/mm^3 because ρ has little effect on the geometric relationship between M_c and S_c, and the minimum value (i.e., 0.01 mm) is predefined considering the size range of d_{3e} (Figure S4). The geometric relationship for the idealized cuboid object (Figure S5) is compared to that for the sampled particles shown in Fig. 3 (Figure S6). The M_c values of 1D and 2D objects vary more as S_c increases, while the variances in M_c of 3D and IS objects are relatively small and constant regardless of S_c. The variance in M_c is mainly caused by the third dimension (i.e., $\log_{10}\rho d_3$; see Table 3). When $S_c = 10^0$ mm^2, the third dimension (d_3) ranges between 0.01 mm and 1 mm. Notably, the minimum value (i.e., 0.01 mm) is predefined, and the maximum value (i.e., 1 mm) is determined to satisfy this requirement: $d_1 \geq d_2 \geq d_3$. The intercepts of Eq. (9) ($\log_{10}\rho d_1$) are approximately between −2 and 0. Furthermore, the slope parameter b depends on morphological characteristics, which range between 1 and 1.5 (Section 4.1). Consequently, M_c varied between the two broken lines shown in Fig. 5, which is a possible range of the geometric relationship. The upper limit is invariant, while the lower limit and the intersection between the two lines depend on the minimum d_3 (0.01 mm in the present study) (Fig. 5). Clearly, the regression line of the sampled MMP particles (*Model* 0; the bold line in Fig. 5) is within the range of possibility.

4.3. Applicability and limitations of the geometric relationship

Our regression models (*Models* 0 to 2) were developed using data for MMP particles with major lengths between 0.3 mm and 25 mm (Fig. 2a). The minimum major length was the mesh size of the plankton net used for sampling, and the upper major length was based on the definition of the mesoplastic size. The major length is commonly used to categorize the size of a plastic but is not correlated with the particle mass because of the absence of second and third dimensions (Figure S2). The particulate mass was strongly correlated with the projected surface area (Fig. 3a). Notably, the variance in the mesoplastic data was similar to that in the microplastic data, implying that the relationship between the mass and the projected surface area of nonvoid plastic particles did not depend on whether the plastics were mesoscale or microscale (Figure S2). Microplastics smaller than 1 mm (SMP) and > 1 mm (LMP) accounted for 28 % and 66 % of the particles (Fig. 2a). Microplastics with these sizes are common in marine environments (Hinata et al., 2023; Isobe et al., 2017; Sagawa et al., 2018). Therefore, our models can be applied to particles in the size range of microplastics collected from marine and river environments.

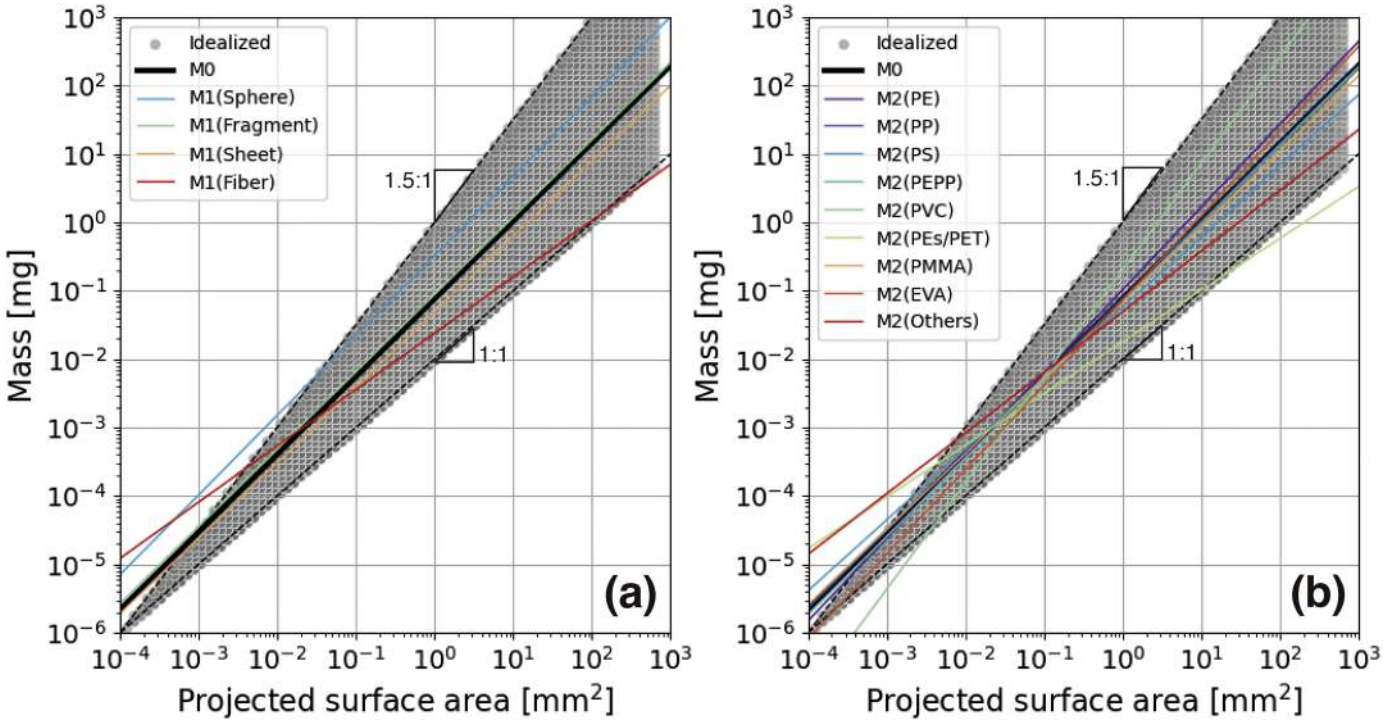

Fig. 5. Comparison between the geometric relationships of the idealized and sampled particles. The gray dots denote the geometric relationship of Mc and *Sc* for the idealized particles, and the broken lines indicate the upper and lower limits of the idealized geometric relationship. The bold solid line indicates the regression line. The colored lines in panels (a) and (b) indicate the regression lines of each shape and polymer type of the sampled particles, respectively.

Nevertheless, there are two limitations of applying the geometric relationship: (1) large uncertainty in the mass estimation of particles with a major-axis length > 10 mm and (2) the quantification of SMPs <10 μm. First, the larger the plastic particles are, the greater the uncertainty in mass estimation because of the variation in the third dimension (Fig. 5). The projected surface area of the sampled particles is distributed between 10^{-2} and 10^{2} mm^2 (Fig. 3b), and 6 % of the mesoplastics (major-axis length of 5–25 mm) are included in the sampled particles (Fig. 2a). Thus, the mass of particles in this size range can be accurately estimated, as shown in Fig. 4. However, our regression models should not be applied to plastic particles with areas larger than the projected surface area of 10^{2} mm^2, such as macroparticles (major-axis length ≥25 mm). Nevertheless, this lack of applicability is not a great issue for the quantification of MMP particles because the masses of large particles can be directly measured.

Second, it is difficult to accurately estimate the masses of plastic particles with a projected surface area <10^{-4} mm^2 because the regression lines exceed the upper limit of the geometric relationship (upper broken line in Fig. 5). Several optical spectroscopies are capable of identifying very tiny plastic particles, while the spatial resolution of optical spectroscopy is limited by the diffraction limit of light in principle. For example, μ-FTIR is regarded as a reliable method for identifying plastic particles larger than 10 μm (10^{-2} mm) (Käppler et al., 2016; Liu et al., 2023). The size of the particles identified by μ-FTIR is applicable to our regression models because the order of magnitude of the projected surface area corresponds to 10^{-4} mm^2. Moreover, μ-Raman has a higher spatial resolution than μ-FTIR, resulting in the detection of relatively small microplastics (Liu et al., 2023). Levermore et al. (2020) reported that μ-Raman spectroscopy is applicable for the direct identification of >2 μm microplastics by optimizing Raman spectral imaging. However, it is necessary to develop a reliable spectroscopic imaging technique to identify microplastics smaller than 10 μm (Levermore et al., 2020). Moreover, our regression models overestimate the masses of SMP particles in the size range, which makes it difficult to estimate the masses of small SMP particles. Instead of optical spectroscopy, pyrolysis gas chromatography/mass spectrometry (Py-GC/MS) might be used for the quantification of small SMP particles. Several researchers have attempted to quantify SMP concentrations by Py-GC/MS (e.g., Lou et al., 2023; Mizuguchi et al., 2023; Morioka et al., 2023). Py-GC/MS is a powerful technique for quantifying SMP in terms of mass concentration and for identifying polymer types without complex pretreatments (Mizuguchi et al., 2023; Morioka et al., 2023). This technique is helpful for overcoming the limitations of SMP quantification derived from optical spectroscopy. Therefore, considering these two limitations, our regression models are applicable to the mass estimation of MMP particles from 10^{-4} mm^2 to 10^{2} mm^2 of the projected surface area.

5. Conclusion

The quantification of the mass concentrations of MMP particles is crucial for assessing the global inventory of ocean plastics and assessing environmental and human health risks. In previous studies, the mass concentration of MMP particles was evaluated by estimating the mass of each particle from its geometric volume assuming a three-dimensional shape. However, the uncertainties in these previous methods for mass estimation have not been sufficiently discussed. Thus, the masses of 4390 MMP particles collected at 35 sites in 17 Japanese rivers from May 2019 to October 2022 were directly measured by an ultramicrobalance. The major shapes were fragmented (70 %) and fibrous (28 %) particles, and the major polymer types were PP (48 %), PE (23 %), and PEs/PET (18 %).

The mass of each particle was linearly regressed on its projected surface area on a log scale. The slope of the regression models was dependent on the three-dimensional shape, which ranged between 1.0 and 1.5 when considering idealized cuboid particles. Moreover, the intercept of the regression models was determined with the geomean of the third dimensions calculated from the mass and projected surface area of the sampled MMP particles regardless of the polymer density. Furthermore, the mass concentrations at the 35 sites were estimated by linear regression models, which resulted in more accurate estimations than those of previous methods based on geometric volume assuming four three-dimensional shapes (i.e., spheres, ellipses, cylinders, and flakes).

Nevertheless, two limitations for mass measurement by linear regression models were identified: (1) large uncertainty in the mass estimation of particles with a major-axis length >10 mm and (2) the quantification of microplastic particles <10 μm. Under these two limitations, linear regression models are applicable for mass estimation of MMP particles in river and marine environments from 10^{-4} mm^2 to 10^{2} mm^2 of the projected surface area. Therefore, our results can be used to accurately estimate the mass concentration in aquatic environments and provide insights into the geometric relationship between the mass and size of MMP particles.

Funding

This work was supported by the Environment Research and Technology Development Fund (JPMEERF21S11900 and JPMEERF20231004) of the Environmental Restoration and Conservation Agency of Japan, KAKENHI (21H01441 and 24K00992), and a project (JPNP18016) commissioned by the New Energy and Industrial Technology Development Organization (NEDO).

CRediT authorship contribution statement

Tomoya Kataoka: Writing – review & editing, Writing – original draft, Visualization, Project administration, Methodology, Investigation, Funding acquisition, Formal analysis, Data curation, Conceptualization. **Yota Iga:** Writing – review & editing, Investigation, Formal analysis, Data curation. **Rifqi Ahmad Baihaqi:** Writing – review & editing, Formal analysis, Data curation. **Hadiyanto Hadiyanto:** Writing – review & editing, Investigation, Formal analysis, Data curation. **Yasuo Nihei:** Writing – review & editing, Project administration, Investigation, Funding acquisition, Data curation.

Declaration of competing interest

No potential conflicts of interest were reported by the authors.

Data availability

Data will be made available on request.

Acknowledgments

The authors are grateful for all the technical staff (Yoriko Murakami and Manami Tanaka at Tokyo University of Science and Hiroko Watanabe at Ehime University) and for their contributions to the laboratory analyses. We would also like to thank the students in the Hydraulics Laboratory of Tokyo University of Science and in the Informatics for Civil Engineering Laboratory of Ehime University for their efforts in the field campaigns. And we would like to thank American Journal Experts (https://www.aje.com/) for English language editing, and also thank anonymous reviewers for their comments to improve the manuscript.

Supplementary materials

Supplementary material associated with this article can be found, in the online version, at doi:10.1016/j.watres.2024.122061.

References

Andrady, A.L., 2017. The plastic in microplastics: a review. Mar. Pollut. Bull. 119 (1), 12–22.

Cózar, A., Echevarría, F., González-Gordillo, J.I., Irigoien, X., Úbeda, B., Hernández-León, S., Palma, Á.T., Navarro, S., García-de-Lomas, J., Ruiz, A., Fernández-de-Puelles, M.L., Duarte, C.M., 2014. Plastic debris in the open ocean. Proc. Natl. Acad. Sci. U.S.A. 111 (28), 10239–10244.

de Ruijter, V.N., Redondo-Hasselerharm, P.E., Gouin, T., Koelmans, A.A., 2020. Quality criteria for microplastic effect studies in the context of risk assessment: a critical review. Environ. Sci. Technol. 54 (19), 11692–11705.

GESAMP, 2019. Guidelines for the monitoring and assessment of plastic litter and microplastics in the ocean. GESAMP Reports and Studies 99, 130.

Hidalgo-Ruz, V., Gutow, L., Thompson, R.C., Thiel, M., 2012. Microplastics in the marine environment: a review of the methods used for identification and quantification. Environ. Sci. Technol. 46 (6), 3060–3075.

Hinata, H., Kuwae, M., Tsugeki, N., Masumoto, I., Tani, Y., Hatada, Y., Kawamata, H., Mase, A., Kasamo, K., Sukenaga, K., Suzuki, Y., 2023. A 75-year history of microplastic fragment accumulation rates in a semi-enclosed hypoxic basin. Sci. Total Environ. 854, 158751.

Isobe, A., Azuma, T., Cordova, M.R., Cózar, A., Galgani, F., Hagita, R., Kanhai, L.D., Imai, K., Iwasaki, S., Kako, S.i., Kozlovskii, N., Lusher, A.L., Mason, S.A., Michida, Y., Mituhasi, T., Morii, Y., Mukai, T., Popova, A., Shimizu, K., Tokai, T., Uchida, K., Yagi, M., Zhang, W., 2021. A multilevel dataset of microplastic abundance in the world's upper ocean and the Laurentian Great Lakes. Microplast. Nanoplast. 1 (1), 16.

Isobe, A., Iwasaki, S., Uchida, K., Tokai, T., 2019. Abundance of non-conservative microplastics in the upper ocean from 1957 to 2066. Nat. Commun. 10 (1), 417.

Isobe, A., Uchiyama-Matsumoto, K., Uchida, K., Tokai, T., 2017. Microplastics in the Southern Ocean. Mar. Pollut. Bull. 114 (1), 623–626.

Iwasaki, S., 2023. Increase in the wave power caused by decreasing sea ice over the Sea of Okhotsk in winter. Sci. Rep. 13 (1), 2539.

Käppler, A., Fischer, D., Oberbeckmann, S., Schernewski, G., Labrenz, M., Eichhorn, K.-J., Voit, B., 2016. Analysis of environmental microplastics by vibrational microspectroscopy: FTIR, Raman or both? Anal. Bioanal. Chem. 408 (29), 8377–8391.

Kataoka, T., Nihei, Y., Kudou, K., Hinata, H., 2019. Assessment of the sources and inflow processes of microplastics in the river environments of Japan. Environ. Pollut. 244, 958–965.

Kataoka, T., Tanaka, M., Mukotaka, A., Nihei, Y., 2023. Experimental uncertainty assessment of meso- and microplastic concentrations in rivers based on net sampling. Sci. Total Environ. 870, 161942.

Koelmans, A.A., Kooi, M., Law, K.L., van Sebille, E., 2017. All is not lost: deriving a top-down mass budget of plastic at sea. Environ. Res. Lett. 12 (11), 114028.

Koelmans, A.A., Redondo-Hasselerharm, P.E., Mohamed Nor, N.H., Kooi, M., 2020. Solving the nonalignment of methods and approaches used in microplastic research to consistently characterize risk. Environ. Sci. Technol. 54 (19), 12307–12315.

Koelmans, A.A., Redondo-Hasselerharm, P.E., Nor, N.H.M., de Ruijter, V.N., Mintenig, S. M., Kooi, M., 2022. Risk assessment of microplastic particles. Nat. Rev. Mater. 7 (2), 138–152.

Kooi, M., Reisser, J., Slat, B., Ferrari, F.F., Schmid, M.S., Cunsolo, S., Brambini, R., Noble, K., Sirks, L.-A., Linders, T.E.W., Schoeneich-Argent, R.I., Koelmans, A.A., 2016. The effect of particle properties on the depth profile of buoyant plastics in the ocean. Sci. Rep. 6 (1), 33882.

Levermore, J.M., Smith, T.E.L., Kelly, F.J., Wright, S.L., 2020. Detection of microplastics in ambient particulate matter using raman spectral imaging and chemometric analysis. Anal. Chem. 92 (13), 8732–8740.

Liu, Z., Wang, W., Liu, X., 2023. Automated characterization and identification of microplastics through spectroscopy and chemical imaging in combination with chemometric: latest developments and future prospects. TrAC Trend. Anal. Chem. 160, 116956.

Lou, F., Wang, J., Sima, J., Lei, J., Huang, Q., 2023. Mass concentration and distribution characteristics of microplastics in landfill mineralized refuse using efficient quantitative detection based on Py-GC/MS. J. Hazard. Mater. 459, 132098.

Michida, Y., Chavanich, S., Cabañas, A.C., Hagmann, P., Hinata, H., Isobe, A., Kershaw, P., Kozlovskii, N., Li, D., Lusher, A.L., Martí, E., Mason, S.A., Mu, J., Saito, H., Shim, W.J., Syakti, A.D., Takada, H., Thompson, R., Tokai, T., Uchida, K., Vasilenko, K., Wang, J., 2019. Guidelines for harmonizing ocean surface microplastic monitoring methods. Ministry Environ. J. (ed) 68.

Mintenig, S.M., Bäuerlein, P.S., Koelmans, A.A., Dekker, S.C., van Wezel, A.P., 2018. Closing the gap between small and smaller: towards a framework to analyse nano- and microplastics in aqueous environmental samples. Environ. Sci. Nano 5 (7), 1640–1649.

Mizuguchi, H., Takeda, H., Kinoshita, K., Takeuchi, M., Takayanagi, T., Teramae, N., Pipkin, W., Matsui, K., Watanabe, A., Watanabe, C., 2023. Direct analysis of airborne microplastics collected on quartz filters by pyrolysis-gas chromatography/mass spectrometry. J. Anal. Appl. Pyrol. 171, 105946.

Morioka, T., Tanaka, S., Yamada, Y., Yukioka, S., Aiba, F., 2023. Quantification of microplastic by particle size down to 1.1 μm in surface road dust in an urban city. Japan. Environ. Pollut. 334, 122198.

Nihei, Y., Ota, H., Tanaka, M., Kataoka, T., Kashiwada, J., 2024. Comparison of concentration, shape, and polymer composition between microplastics and mesoplastics in Japanese river waters. Water Res 249, 120979.

Nihei, Y., Yoshida, T., Kataoka, T., Ogata, R., 2020. High-resolution mapping of Japanese microplastic and macroplastic emissions from the land into the Sea. Water (Basel) 12 (4).

Pabortsava, K., Lampitt, R.S., 2020. High concentrations of plastic hidden beneath the surface of the Atlantic ocean. Nat. Commun. 11 (1), 4073.

Poulain, M., Mercier, M.J., Brach, L., Martignac, M., Routaboul, C., Perez, E., Desjean, M. C., ter Halle, A., 2019. Small microplastics as a main contributor to plastic mass balance in the north atlantic subtropical Gyre. Environ. Sci. Technol. 53 (3), 1157–1164.

Redondo-Hasselerharm, P.E., Falahudin, D., Peeters, E.T.H.M., Koelmans, A.A., 2018. Microplastic effect thresholds for freshwater benthic macroinvertebrates. Environ. Sci. Technol. 52 (4), 2278–2286.

Rosal, R., 2021. Morphological description of microplastic particles for environmental fate studies. Mar. Pollut. Bull. 171, 112716.

Sagawa, N., Kawaai, K., Hinata, H., 2018. Abundance and size of microplastics in a coastal sea: comparison among bottom sediment, beach sediment, and surface water. Mar. Pollut. Bull. 133, 532–542.

Senathirajah, K., Attwood, S., Bhagwat, G., Carbery, M., Wilson, S., Palanisami, T., 2021. Estimation of the mass of microplastics ingested – a pivotal first step towards human health risk assessment. J. Hazard. Mater. 404, 124004.

Simon, M., van Alst, N., Vollertsen, J., 2018. Quantification of microplastic mass and removal rates at wastewater treatment plants applying Focal Plane Array (FPA)-based Fourier Transform Infrared (FT-IR) imaging. Water Res 142, 1–9.

Tagg, A.S., Harrison, J.P., Ju-Nam, Y., Sapp, M., Bradley, E.L., Sinclair, C.J., Ojeda, J.J., 2017. Fenton's reagent for the rapid and efficient isolation of microplastics from wastewater. Chem. Comm. 53 (2), 372–375.

Tanaka, M., Kataoka, T., Nihei, Y., 2022. Variance and precision of microplastic sampling in urban rivers. Environ. Pollut. 310, 119811.

Tanaka, M., Kataoka, T., Nihei, Y., 2023. An analytical approach to confidence interval estimation of river microplastic sampling. Environ. Pollut. 335, 122310.

Thompson, R.C., Olsen, Y., Mitchell, R.P., Davis, A., Rowland, S.J., John, A.W.G., McGonigle, D., Russell, A.E., 2004. Lost at sea: where is all the plastic? Science 304.

Tötzke, C., Oswald, S.E., Hilger, A., Kardjilov, N., 2021. Non-invasive detection and localization of microplastic particles in a sandy sediment by complementary neutron and X-ray tomography. J. Soils Sediments 21 (3), 1476–1487.

Yokota, K., Waterfield, H., Hastings, C., Davidson, E., Kwietniewski, E., Wells, B., 2017. Finding the missing piece of the aquatic plastic pollution puzzle: interaction between primary producers and microplastics. Limnol. Oceanogr. Lett. 2 (4), 91–104.